Dynamic effects in electron momentum spectroscopy of sulfur hexafluoride

Xing Wang,[1] Shenyue Xu,[1] Chuangang Ning,[2,*] O. Al-Hagan,[3,4] Pengfei Hu,[1] Yongtao Zhao,[1] Zhongfeng Xu,[1,†] Jingkang Deng,[2] Enliang Wang,[5] Xueguang Ren,[1,5,‡] Alexander Dorn,[5] and Don Madison[3]

[1]*School of Science, Xi'an Jiaotong University, 710049 Xi'an, China*

[2]*Department of Physics, State Key Laboratory of Low-Dimensional Quantum Physics, Tsinghua University, Beijing 100084, China*

[3]*Physics Department, Missouri University of Science and Technology, Rolla, Missouri 65409, USA*

[4]*Department of Physics, King Khalid University, Abha 61421, Saudi Arabia*

[5]*Max-Planck-Institut für Kernphysik, 69117 Heidelberg, Germany*

(Received 19 February 2018; revised manuscript received 14 May 2018; published 18 June 2018)

Electron momentum spectroscopy (EMS) results are presented for the sulfur hexafluoride (SF_6) molecule using a high-resolution binary $(e, 2e)$ spectrometer at incident energies (E_i) of 600, 1200, and 2400 eV plus the binding energy. The valence orbital momentum profiles were measured with a binding energy resolution of 0.68 eV and angular resolutions of $\Delta\theta = \pm 0.6^\circ$, $\Delta\phi = \pm 0.85^\circ$. Whereas the two higher incident energies are in the range where normally EMS measurements do not exhibit an impact-energy dependence, the current experimental data display a dynamic dependence on the impact energies. The measured momentum profiles are compared with predictions from a plane-wave impulse approximation (PWIA) calculation using molecular orbitals obtained from a density-functional-theory quantum-chemistry calculation. The PWIA calculations are in fairly good agreement with experiment only for 2400 eV impact energy, particularly for the summed $1t_{2u}$ and $5t_{1u}$ orbitals. We have also compared the experimental results for the $5a_{1g}$ state with the molecular three-body distorted-wave (M3DW) approach using the orientation-averaged molecular orbital approximation. Unlike the PWIA, the M3DW results are in very good agreement with the experimental data at all three measured incident energies for small momenta, which indicates that dynamical distortion effects are important for this molecule.

DOI: 10.1103/PhysRevA.97.062704

I. INTRODUCTION

It is now well documented that electron momentum spectroscopy (EMS) serves as a sensitive probe of the electronic structure of atoms and molecules [1–4]. The EMS process is electron-impact ionization of the target where the projectile electron and ionized electron are detected in coincidence. The standard impact-energy range for these experiments is 1–2 keV [2]. The residual ion acts as a spectator; the target electron momentum p is equal in magnitude but opposite in sign to the recoil ion momentum. Within the plane-wave impulse approximation (PWIA), the measured $(e,2e)$ cross section is directly proportional to the momentum-space wave function of the ionized electron [1–4]. As a result, the measured cross sections do not depend on the incident-electron impact energy.

Many experimental and theoretical works have shown that the PWIA is usually valid for impact energies in the keV range [1,2]. However, it was recently found that the PWIA is not valid for some cases, e.g., ionization of the atomic nd orbitals [5,6], the $^2\Pi_g$ orbital in molecular oxygen (O_2) [7], the $1E_g$ orbital in ethane (C_2H_6) [8], and the $1b_{3g}$ orbital in ethylene (C_2H_4) [9]. For these cases, experiment found a higher intensity than was predicted by the PWIA in the low-momentum region, as well as an impact-energy-dependent effect. For atomic orbitals, the observed higher intensity at low momenta can be well reproduced by distorted-wave calculations [5,6,10]. For molecules, calculations considering molecular vibration indicate that the higher intensity at the low momenta can be partly, but not totally, attributed to vibrational effects; see, e.g., [11–13].

Recently, the Hefei EMS group [14] and Sendai EMS group [15] have performed experiments on sulfur hexafluoride (SF_6) at the impact energy of ∼1200 eV to study the interference effect or bond oscillation for the five outermost molecular orbitals of SF_6, which are each constructed from the $2p$ atomic orbital of the F atoms. The experimental momentum distributions show higher intensity at the low-momentum region than predicted by the PWIA calculations. This increased low-momentum intensity has been labeled the "turn-up" effect in EMS [5,7,9]. Even considering the vibrational effects, the turn-up effect has not been satisfactorily explained [15]. An open question then is whether this observed effect can be explained by distortions of the continuum wave functions which has not yet been investigated.

In the present work, we conducted high-resolution EMS experiments for the valence orbitals of SF_6 at various projectile energies of ∼600, ∼1200, and ∼2400 eV in order to examine the validity of the PWIA and the influence of the distorted-wave effects. Momentum profiles for the $1t_{1g}$, $1t_2u{+}5t_{1u}$, $3e_g$, $1t_{2g}$, $4t_{1u}$, and $5a_{1g}$ states were obtained and compared with the PWIA calculations. The experimental data show higher intensity than the PWIA in the low-momentum region and a dynamic dependence on the impact energies also

*Corresponding author: ningcg@mail.tsinghua.edu.cn
†Corresponding author: zhfxu@mail.xjtu.edu.cn
‡Corresponding author: renxueguang@xjtu.edu.cn

contrary to the PWIA calculations. Distorted-wave calculations were performed for ionization of the $5a_{1g}$ state using the molecular three-body distorted-wave (M3DW) approach with the orientation-averaged molecular orbital (OAMO) approximation. Both the low-momentum intensity and energy dependence of the data are rather well reproduced by the M3DW. It is rarely reported that the distorted-wave method is utilized to model the EMS measurements of the bound electron momentum profile for molecular orbitals.

This paper is organized as follows. After a brief description of the experimental apparatus in Sec. II, we summarize the essential points of the two theoretical models in Sec. III. The results are presented and discussed in Sec. IV before we finish with the conclusions in Sec. V.

II. EXPERIMENTAL METHOD

The experiment was performed using a high-resolution and high-efficiency electron momentum spectrometer. The detail of this apparatus has been reported in previous works [16–19] and hence will not be repeated here. Briefly, it utilizes a noncoplanar symmetric geometry, i.e., the two outgoing electrons have almost equal energies and equal polar angles ($\theta_a \approx \theta_b = 45^\circ$) with respect to the direction of the incident electron beam. A double-toroidal energy analyzer equipped with two large position-sensitive detectors was used to detect the two outgoing electrons in coincidence. This spectrometer can collect the multienergy and multiangle electrons simultaneously, thus the detection efficiency of the coincidence (e, $2e$) events was greatly increased. An electron gun equipped with an oxide cathode was designed to produce the electron beam with a low-energy spread and low divergence angle. Compared to the generic filament cathodes, the oxide cathode can work at a much lower temperature (~1100 K), and thus a small energy spread of the electron beam can be achieved. The electron-beam size was constrained to 0.3 mm in diameter by a molybdenum aperture. The binding-energy resolution in the present work is 0.68 eV, and angular resolutions are $\Delta\theta = \pm 0.6^\circ$, $\Delta\phi = \pm 0.85^\circ$, respectively, which were obtained with the calibration measurements of helium and argon. A commercial SF_6 gas sample with 99.9% purity was used in the experiment.

Using energy and momentum conservation, the binding energies ε and momenta p of the bound electron prior to being ejected can be determined. This momentum p is dependent on the out-of-plane azimuthal angle ϕ between the two outgoing electrons:

$$p = \sqrt{(p_i - \sqrt{2}p_a)^2 + 2p_a^2 \sin^2(\phi/2)}, \tag{1}$$

where p_i and p_a ($p_a = p_b$) are the momenta of the incident electron and the outgoing electrons, respectively.

III. THEORETICAL MODELS

Within the plane-wave impulse approximation (PWIA) framework, and the target Hartree-Fock approximation (THFA) or the target Kohn-Sham approximation (TKSA), the triple-differential cross section (TDCS) for randomly oriented molecules is given by

$$\frac{d^3\sigma}{d\Omega_a d\Omega_b dE_b} \propto S_i^f \int d\Omega |\psi_i(p)|^2, \tag{2}$$

where $\psi_i(p)$ is the momentum-space representation of a canonical Hartree-Fock or Kohn-Sham orbital wave function, and S_i^f denotes the associated spectroscopic factor, which accounts for the shake-up processes due to configuration interactions in the final state, and $\int d\Omega$ denotes the spherical average over the random molecular orientations. The molecular orbitals were calculated using a density-functional-theory (DFT) program along with the standard hybrid functional B3LYP with TZ2P Slater-type basis set in the Amsterdam density functional (ADF) program. The resulting molecular orbitals were used to generate the theoretical momentum-space wave function using our recently developed program named NEMS [20], which formally can process any type (s,p,d,f,g ...) of atomic orbital wave functions.

It should be noted that the distortion interactions for all continuum electron wave functions are neglected in the PWIA calculation. To consider the distorted-wave effects, the molecular three-body distorted-wave (M3DW) calculation with the orientation-averaged molecular orbital approximation is used to describe the present electron-impact ionization process. Although the M3DW has been described previously [21–24], we summarize the essential ideas and the particular ingredients for the current cases of interest in order to make this paper self-contained. More detailed information can be found in the given references. The direct-scattering amplitude is given by

$$T_{\rm dir} = \langle \chi_a^-(\boldsymbol{k}_a,\boldsymbol{r}_0)\chi_b^-(\boldsymbol{k}_b,\boldsymbol{r}_1)C_{ab}(\boldsymbol{r}_{01})|W| \times \phi_{DY}(\boldsymbol{R},\boldsymbol{r}_1)\chi_i^+(\boldsymbol{k}_i,\boldsymbol{r}_0)\rangle, \tag{3}$$

where $\boldsymbol{k}_i$,$\boldsymbol{k}_a$, and $\boldsymbol{k}_b$ are the wave vectors for the initial, scattered, and ejected electrons, respectively, $\chi_i^+(\boldsymbol{k}_i,\boldsymbol{r}_0)$ is an initial-state continuum distorted wave and the (+) indicates outgoing wave boundary conditions, $\chi_a^-(\boldsymbol{k}_a,\boldsymbol{r}_0)$,$\chi_b^-(\boldsymbol{k}_b,\boldsymbol{r}_1)$ are the scattered and ejected electron distorted waves with incoming wave boundary conditions, and the factor $C_{ab}(\boldsymbol{r}_{01})$ is the final-state Coulomb-distortion factor between the two electrons, normally called the postcollision interaction (PCI). Here we use the exact final-state electron-electron interaction and not an approximation for it such as the Ward-Macek factor [25]. The perturbation $W = V_i - U_i$, where V_i is the initial-state interaction potential between the incident electron and the neutral molecule, and U_i represents the initial-state spherically symmetric approximation for V_i and U_i, is used to calculate the initial-state distorted wave $\chi_i^+(\boldsymbol{k}_i,\boldsymbol{r}_0)$. Here, $\phi_{DY}(\boldsymbol{R},\boldsymbol{r}_1)$ is the initial bound-state molecular wave function, which is commonly called the Dyson molecular orbital, for the active electron and it depends both on the electron coordinate $\boldsymbol{r_1}$ and the orientation of the molecule, which is designated by $\boldsymbol{R}$. The triple differential cross section (TDCS) for a given orientation $\boldsymbol{R}$ with respect to the laboratory frame can be obtained from

$$\sigma^{\rm TDCS}(\boldsymbol{R}) = \frac{1}{(2\pi)^5}\frac{k_a k_b}{k_i}[|T_{\rm dir}(\boldsymbol{R})|^2 + |T_{\rm exc}(\boldsymbol{R})|^2 + |T_{\rm dir}(\boldsymbol{R}) - T_{\rm exc}(\boldsymbol{R})|^2], \tag{4}$$

where the exchange-scattering T_{exc} is calculated similar to T_{dir}, except that the particles 1 and 2 are interchanged in the final-state wave function. The only term in the integral for the T matrix that depends on the orientation is the Dyson wave function. In the OAMO orientation-averaged molecular orbital (OAMO) approximation [21,22], we average the wave function over all orientations and then we calculate a single TDCS. This approximation makes these calculations tractable with present computing resources.

The important differences between the PWIA and the M3DW are the following. In the PWIA, all continuum-state electron wave functions are treated as plane waves and the postcollision interaction is treated only to first order. In the M3DW, all continuum electron wave functions are distorted waves. A distorted wave is a numerical wave function that is a solution of the Schrödinger equation for a numerical-distorting potential calculated based upon the location of all the atomic nuclei and the electronic charge density of the molecule. For the interaction between the continuum electron and the bound electrons, the molecular electronic charge density is averaged over all orientations and then it is used to calculate the radially dependent potential between the bound electrons and the continuum electron. For the interactions with the atomic nuclei, each nuclei is averaged over all orientations, which means that each nuclear charge is effectively placed on a sphere centered on the center of mass. For SF_6, this means that there is a charge of 16 (sulfur) at the center of mass and a charge of 54 on a sphere of radius 3 a.u. since all six fluorine nuclei are almost the same distance from the center of mass. When the electronic and nuclear parts are combined, we have a screened potential which, for a fixed radius, corresponds to a potential equivalent to the net charge inside a sphere of that radius. For the incoming electron, the asymptotic form of this potential is zero and, for the two outgoing electrons, the asymptotic form of this potential corresponds to an effective charge of +1. The other important difference between the PWIA and the M3DW is that the M3DW has the postcollision interaction to all orders of perturbation theory instead of just to the first order. This will be important for equal energy electrons leaving the collision at small angular separations, but probably is not important for the present kinematics.

IV. RESULTS AND DISCUSSIONS

SF_6 has an octahedral geometry, O_h symmetry, consisting of six fluorine atoms attached to a central sulfur atom. Within Hartree-Fock theory, the ground-state configuration can be written as $(\text{core})^{22}(4a_{1g})^2(3t_{1u})^6(2e_g)^4(5a_{1g})^2(4t_{1u})^6(1t_{2g})^6(3e_g)^4(5t_{1u})^6(1t_{2u})^6(1t_{1g})^6$.

Figure 1 presents the measured binding-energy spectra of SF_6. Here, the binding energy ε is equal to the incident electron energy minus the two outgoing electron energies ($\varepsilon = E_i - E_a - E_b$). The outer valence orbitals of SF_6 are well resolved in the binding-energy spectrum, except for the overlap of $5t_{1u}$ and $1t_{2u}$, which cannot be resolved even with the high-resolution photoelectron spectroscopy (PES) [26]. The binding-energy spectra at different ϕ angles can be obtained simultaneously using the spectrometer. From the angle-energy density map displayed in Fig. 1(a), the basic features of EMS for each orbital

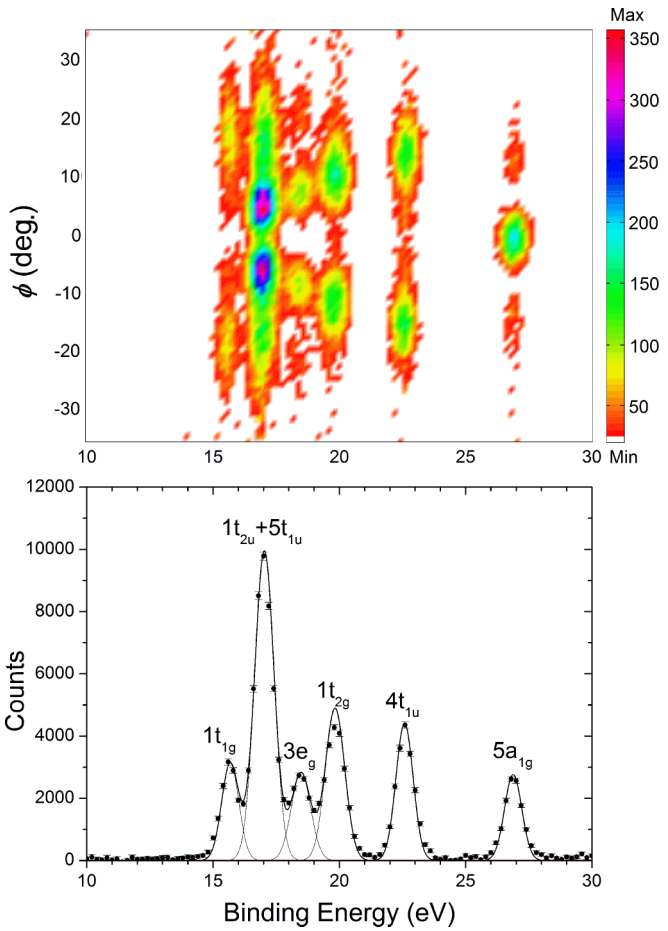

FIG. 1. Momentum-energy density map of SF_6 (top) and binding-energy spectrum summed over all azimuthal angles ϕ (bottom), obtained at the impact energy of 1200 eV plus binding energies. The dashed lines represent Gaussian fits to the individual peaks and the solid curve is the summed fit. The labels of each peak are the orbital assignment.

can be seen directly. Density minima are observed for each orbital at the azimuthal angle $\phi = 0^\circ$ ($p \approx 0$), except for the $5a_{1g}$ orbital because the S $2s$ state contributes to the $5a_{1g}$ orbital while the others contain mainly the F $2p$ state. The binding-energy spectrum in the bottom panel of Fig. 1 was obtained by summing all the energy spectra for different ϕ angles. To obtain the experimental momentum distribution for each orbital, the binding-energy spectra at the different ϕ angles were fitted with the multiple Gaussian functions. The peak centers were determined through high-resolution PES, and the widths were determined by combining the experimental energy resolution and the vibrational broadening on PES. The experimental momentum distributions were obtained by fitting the intensity for each state plotted as a function of the momentum p.

To compare the experimental momentum distributions with theory, a normalization procedure is needed because the experimental intensity is on a relative scale. A global normalization factor was determined by fitting the summed experimental momentum distributions in Fig. 1 to the corresponding PWIA distributions, i.e., $5a_{1g}+4t_{1u}+1t_{2g}+3e_g+5t_{1u}+1t_{2u}+1t_{1g}$, and then this factor was used to normalize the experimental

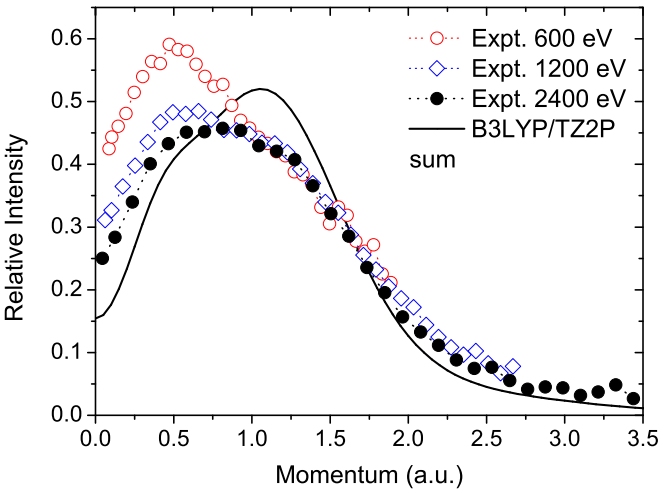

FIG. 2. Measured and PWIA-calculated spherically averaged momentum profiles for the sum of $5a_{1g}+4t_{1u}+1t_{2g}+3e_g+5t_{1u}+1mt_{2u}+1t_{1g}$ orbitals of SF_6 at the impact energies of 600, 1200, and 2400 eV. The solid line is the PWIA results with the DFT-B3LYP/TZ2P method.

distributions for each orbital. As Fig. 2 shows, the experimental distributions for different impact energies agree well with each other for the momentum region $p > 1.0$ a.u., therefore the data in this region were used to determine the normalization factor. The best fit to the experimental data in this region of momenta was obtained by normalizing the data to the PWIA at p about 1.5 a.u. From Fig. 2, one can also see an energy-dependent effect for $p < 1.0$ a.u. Below we will discuss this structure in more detail for the individual orbitals.

The experimental momentum distributions for projectile energies of 600, 1200, and 2400 eV are compared in Figs. 3(a)–3(f) with the PWIA calculations for the states $1t_{1g}$, $5t_{1u}+1t_{2u}$, $3e_g$, $1t_{2g}$, $4t_{1u}$, and $5a_{1g}$, respectively. The experimental data are generally well described by PWIA in the high-momentum range ($p > 1.0$ a.u.). However, at low momenta ($p < 1.0$ a.u.), there is an unexpected higher intensity observed compared to PWIA, which has been called the turn-up effect. Such turn-up effects can be qualitatively explained by the distortion of the incoming and outgoing electron waves in the target and the ion potentials since the size of the effect decreases with increasing impact energy [5]. For most cases, the turn-up effect occurs in the low-momentum range and is most evident at impact energy of 600 eV, becomes smaller at 1200 eV, and is much smaller at 2400 eV. Particularly for the summed $1t_{2u}$ and $5t_{1u}$ orbitals shown in Fig. 3(b), both experiment and the PWIA have a maximum intensity at $p \sim 0.5$ a.u. and a second shoulder structure at $p \sim 1.5$ a.u. For this case, the increased intensity is seen at the peak ($p \sim 0.5$ a.u.). Increased intensity at low momenta has been observed in the atomic nd orbitals where the distorted-wave impulse approximation (DWIA) calculations supported the idea that the turn-up effect at low momenta is due to distorted-wave effects [5]. Further analysis of the orbital symmetry indicates that the low momenta can contribute to the electron density in the near nuclear region in d orbitals where distortion effects should be the strongest. The DWIA calculations for atomic nd orbitals at 600, 1200, and

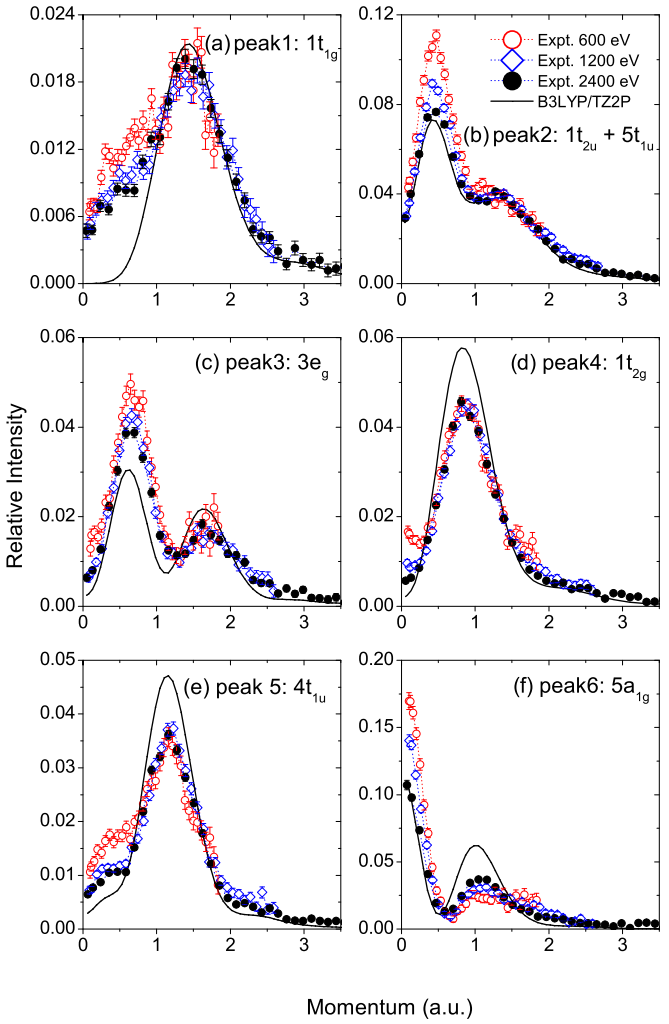

FIG. 3. Measured and PWIA-calculated spherically averaged momentum profiles for the outer valence orbitals of SF_6: (a) $1t_{1g}$, (b) $5t_{1u}+1t_{2u}$, (c) $3e_g$, (d) $1t_{2g}$, (e) $4t_{1u}$, (f) $5a_{1g}$ at impact energies of 600, 1200, and 2400 eV. The solid lines are PWIA-calculated results with the DFT-B3LYP/TZ2P method, which have been convolved with the experimental resolution at 2400 eV.

2400 eV confirmed that such distortion effects should decrease with increasing impact energy [5]. Unfortunately, theoretical calculations using the DWIA for molecules have not been reported so far.

For the $1t_{1g}$, $3e_g$, $1t_{2g}$, and $4t_{1u}$ orbitals, the deviations between the experimental distributions and PWIA at low momenta decrease with increasing impact energy. However, the agreements between the experimental data and PWIA for 2400 eV are not as good as is seen for the case of the $1t_{2u}+5t_{1u}$ orbitals. The influence of molecular vibration is a possible source of the observed disagreement for low momenta, which has been analyzed by Watanabe *et al.* [15]. It was found that for the $1t_{1g}$ orbital, the vibrational-effects calculation predicts higher intensity than the equilibrium geometry calculation for low momenta, which reduced the deviation (~50%) from the experimental result. While there are no noticeable differences between the two kinds of calculations for the $3e_g$ and $1t_{2g}$ orbitals, showing that influence of nuclear motion on their

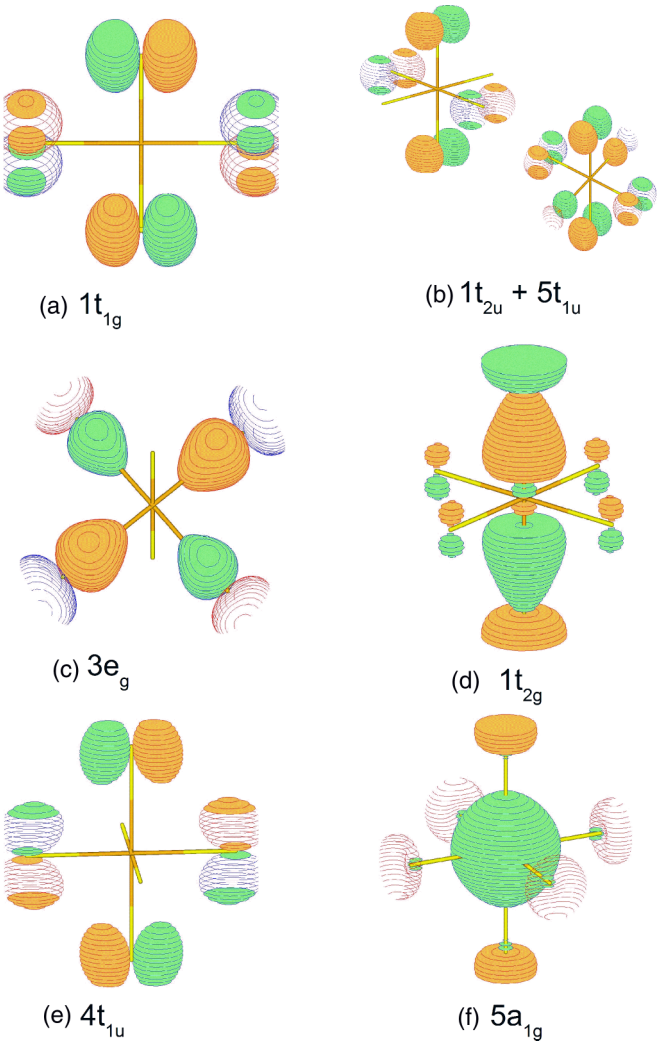

FIG. 4. The molecular orbital patterns of SF_6 with density contour value 0.1.

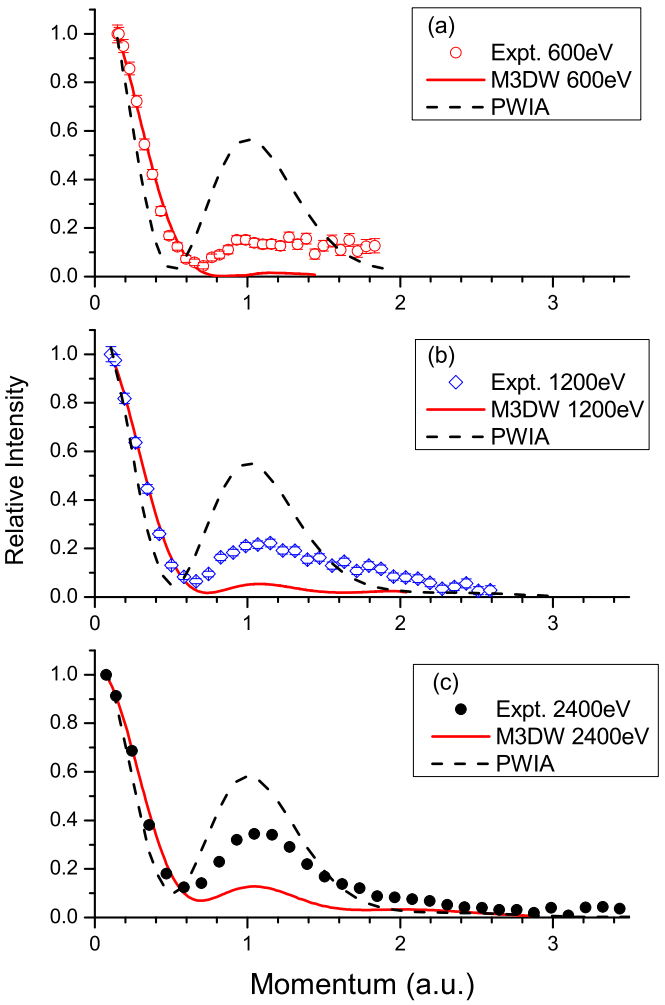

FIG. 5. The comparison of measured, and PWIA- and M3DW-calculated momentum profiles for the $5a_{1g}$ orbital at the impact energies of 600, 1200, and 2400 eV. The results are normalized to unity at $p \approx 0$ a.u.

electron momentum distributions probably cannot explain this effect. Other effects, such as dynamic correlation, have been mentioned in the literature [7] as a possible reason for the higher intensity at low momenta in the experiment.

The PWIA theory predicted a $s - p$-type momentum distribution for the $5a_{1g}$ orbital [Fig. 3(f)], which is generally consistent with the shape of the experimental distributions. We now focus on the results of the $5a_{1g}$ orbital since the M3DW calculations can be performed for this orbital. Figure 4 shows the molecular orbitals for SF_6. It can be seen from Fig. 4 that except for the $5a_{1g}$ orbital, all other orbitals will produce a zero wave function with the OAMO approximation due to the antisymmetry. Thus, only the $5a_{1g}$ orbital can be calculated using the M3DW model. In Fig. 5, the M3DW results are compared with experiment and the PWIA, where both theory and experiment are normalized to unity at $p \approx 0$ a.u. As can be seen from the figure, the M3DW is in reasonably good agreement with experiment for low momenta for all three impact energies. The PWIA, on the other hand, is the same for all energies and agrees best with the data for the highest energy. The M3DW results are not in very good agreement with experiment for the peak observed near a momentum of unity. However, this is a well-known problem associated with the OAMO approximation for lower-energy TDCS work. In the PWIA, the momentum is equal (in magnitude) to the momentum of the recoil ion. The low-energy TDCS results have a peak (called the binary peak) which would correspond to low recoil ion momenta and a second much smaller peak (called the recoil peak) which would correspond to high recoil ion momenta. The OAMO results typically are in reasonably good agreement with the binary peak and significantly underestimate the recoil peak (very similar to the results seen in Fig. 5) [27–32]. In spite of the fact that the M3DW underestimates the observed peak at p around 1.1 a.u., it is interesting to note that M3DW predicted the same trend for the impact-energy dependence of the 1.1 a.u. intensity as the experimental observation with the intensity increasing with increasing energy.

The most likely problem with the OAMO approximation can be seen from an examination of the $5a_{1g}$ wave function. As Fig. 4(f) shows, there are six antisymmetric lobes, which will produce zero intensity at a larger-r region with OAMO approximation. The central ball in the $5a_{1g}$ orbital is mainly

attributed to the S $2s$ electron, while the six outer lobes are from the F $2p$ and $2s$ electrons. Molecular orbital population analysis predicted that the S $2s$ contributes about 33% of the gross orbital electron density, while the contribution from the F atoms is 67%. The OAMO approximation probably underestimates the contributions from the six F atoms, which are mainly at $p \approx 1$ a.u. Recent $(e, 2e)$ studies of CH_4 [33] and H_2O [34] indicate that it is more accurate to perform a proper average (PA) over orientation-dependent cross sections than to use the OAMO. The computational cost of the PA method, however, is much higher than the OAMO and we do not presently have sufficient computational resources to perform a PA calculation for energies this high. A recent multicenter distorted-wave (MCDW) method [35–37] developed for high-impact energies is expected to become a suitable model for EMS for investigating the distorted-wave effect in the future.

In the M3DW model, the continuum wave functions (distorted waves) are elastic-scattering waves. The potential used for calculating the elastic scattering is composed of a spherically symmetric electronic part plus nuclear part. For the nuclear part, the spherical average places the charge of the nucleus on a thin ball with a radius equal to the distance of the nuclei from the center of mass. Another possible reason for the discrepancy with experiment is that the spherical averaging process reduces the strength of the elastic scattering from the nuclei too much. If this is the case, a similar phenomenon should also be seen in highly symmetric molecules, such as carbon tetrachloride. High-resolution $(e, 2e)$ experiments for these molecules are under preparation at various impact energies.

V. CONCLUSIONS

We have reported a combined experimental and theoretical study of electron momentum spectroscopy of sulfur hexafluoride (SF_6). The electron momentum profiles of SF_6 valence orbitals were measured using a high-resolution binary $(e, 2e)$ spectrometer at various projectile energies of 600, 1200, and 2400 eV. The binding-energy resolution of $\Delta\varepsilon = 0.68$ eV allows us to nicely resolve all the valence orbitals, except for the overlap of the $5t_{1u}$ and $1t_{2u}$ orbitals. The purpose of this study was to provide a direct test of the distorted-wave effect as a function of impact energy.

The experimental momentum distributions for the individual orbitals were compared with plane-wave impulse approximation results and it was found that the experimental data are generally well described by the PWIA in the high-momentum range ($p > 1.0$ a.u.). For low momenta, the experimentally observed intensity was higher than expected and also showed an energy dependence not predicted by the PWIA. This discrepancy can be qualitatively explained by the distortion of the incoming and outgoing electron waves in the target and the ion potentials. This explanation is supported by the fact that the discrepancy between experiment and theory decreases with increasing impact energy, particularly for the summed $1t_{2u}$ and $5t_{1u}$ momentum profile. Additionally, the higher intensity at low momenta for the low-impact energy of 600 eV becomes smaller at 1200 eV, and, for most cases, is either small or gone when the projectile energy is further increased to 2400 eV.

Distorted-wave calculations for electron momentum spectroscopy of molecules were reported using the molecular three-body distorted-wave approach coupled with the orientation-averaged molecular orbital approximation for the $5a_{1g}$ orbital of SF_6. Unlike the PWIA, the M3DW properly predicts the low-momentum features and energy-dependent change in the momentum profiles. This is a direct demonstration of the influence of distorted-wave effects on the momentum profiles for molecules.

ACKNOWLEDGMENTS

This work was supported, in part, by Science Challenge Project under Grant No. TZ2016005, the National Natural Science Foundation of China under Grants No. 11774281 and No. U1532263, Project of Thousand Youth Talents in China, and the US National Science Foundation under Grant No. 1505819. E.W. acknowledges financial support through a fellowship from the Alexander von Humboldt Foundation.

[1] C. E. Brion, Int. J. Quantum Chem. **29**, 1397 (1986).
[2] I. E. McCarthy and E. Weigold, Rep. Prog. Phys. **54**, 789 (1991).
[3] M. A. Coplan, J. H. Moore, and J. P. Doering, Rev. Mod. Phys. **66**, 985 (1994).
[4] M. Takahashi, Bull. Chem. Soc. Jpn. **82**, 751 (2009).
[5] C. E. Brion, Y. Zheng, J. Rolke, J. J. Neville, I. E. McCarthy, and J. Wang, J. Phys. B **31**, L223 (1998).
[6] X. G. Ren, C. G. Ning, J. K. Deng, G. L. Su, S. F. Zhang, and Y. R. Huang, Phys. Rev. A **73**, 042714 (2006).
[7] C. G. Ning, X. G. Ren, J. K. Deng, G. L. Su, S. F. Zhang, and G. Q. Li, Phys. Rev. A **73**, 022704 (2006).
[8] X. Ren, C. Ning, J. Deng, S. Zhang, G. Su, Y. Huang, and G. Li, J. Electron Spectrosc. Relat. Phenom. **151**, 92 (2006).
[9] X. G. Ren, C. G. Ning, J. K. Deng, S. F. Zhang, G. L. Su, F. Huang, and G. Q. Li, Phys. Rev. Lett. **94**, 163201 (2005).
[10] C. D. Cappello, F. Menas, S. Houamer, Y. V. Popov, and A. C. Roy, J. Phys. B **48**, 205201 (2015).
[11] N. Watanabe, M. Yamazaki, and M. Takahashi, J. Chem. Phys. **137**, 114301 (2012).
[12] F. Morini, N. Watanabe, M. Kojima, M. S. Deleuze, and M. Takahashi, J. Chem. Phys. **146**, 094307 (2017).
[13] Y. Tang, X. Shan, J. Yang, S. Niu, Z. Zhang, N. Watanabe, M. Yamazaki, M. Takahashi, and X. Chen, J. Phys. Chem. A **120**, 6855 (2016).
[14] M.-F. Zhao, X. Shan, J. Yang, E.-L. Wang, S.-S. Niu, and X.-J. Chen, Chin. J. Chem. Phys. **28**, 539 (2015).
[15] N. Watanabe, M. Yamazaki, and M. Takahashi, J. Electron Spectrosc. Relat. Phenom. **209**, 78 (2016).
[16] X. G. Ren, C. G. Ning, J. K. Deng, S. F. Zhang, G. L. Su, F. Huang, and G. Q. Li, Rev. Sci. Instrum. **76**, 063103 (2005).
[17] X.-G. Ren, C.-G. Ning, J.-K. Deng, S.-F. Zhang, G.-L. Su, B. Li, and X.-J. Chen, Chin. Phys. Lett. **22**, 1382 (2005).
[18] C.-G. Ning, S.-F. Zhang, J.-K. Deng, K. Liu, Y.-R. Huang, and Z.-H. Luo, Chin. Phys. B **17**, 1729 (2008).

[19] C. G. Ning, J. K. Deng, G. L. Su, H. Zhou, and X. G. Ren, Rev. Sci. Instrum. **75**, 3062 (2004).
[20] C. Ning, B. Hajgat, Y. Huang, S. Zhang, K. Liu, Z. Luo, S. Knippenberg, J. Deng, and M. Deleuze, Chem. Phys. **343**, 19 (2008).
[21] J. Gao, J. L. Peacher, and D. H. Madison, J. Chem. Phys. **123**, 204302 (2005).
[22] D. H. Madison and O. Al-Hagan, J. At. Mol. Opt. Phys. **2010**, 367180 (2010).
[23] K. L. Nixon, A. J. Murray, H. Chaluvadi, S. Amami, D. H. Madison, and C. Ning, J. Chem. Phys. **136**, 094302 (2012).
[24] C. J. Colyer, M. A. Stevenson, O. Al-Hagan, D. H. Madison, C. G. Ning, and B. Lohmann, J. Phys. B **42**, 235207 (2009).
[25] S. J. Ward and J. H. Macek, Phys. Rev. A **49**, 1049 (1994).
[26] D. Holland, M. MacDonald, P. Baltzer, L. Karlsson, M. Lundqvist, B. Wannberg, and W. von Niessen, Chem. Phys. **192**, 333 (1995).
[27] J. D. Builth-Williams, S. M. Bellm, D. B. Jones, H. Chaluvadi, D. H. Madison, C. G. Ning, B. Lohmann, and M. J. Brunger, J. Chem. Phys. **136**, 024304 (2012).
[28] S. M. Bellm, J. D. Builth-Williams, D. B. Jones, H. Chaluvadi, D. H. Madison, C. G. Ning, F. Wang, X. G. Ma, B. Lohmann, and M. J. Brunger, J. Chem. Phys. **136**, 244301 (2012).
[29] J. D. Builth-Williams, S. M. Bellm, L. Chiari, P. A. Thorn, D. B. Jones, H. Chaluvadi, D. H. Madison, C. G. Ning, B. Lohmann, G. B. da Silva, and M. J. Brunger, J. Chem. Phys. **139**, 034306 (2013).
[30] J. D. Builth-Williams, G. B. da Silva, L. Chiari, D. B. Jones, H. Chaluvadi, D. H. Madison, and M. J. Brunger, J. Chem. Phys. **140**, 214312 (2014).
[31] G. B. da Silva, R. F. C. Neves, L. Chiari, D. B. Jones, E. Ali, D. H. Madison, C. G. Ning, K. L. Nixon, M. C. A. Lopes, and M. J. Brunger, J. Chem. Phys. **141**, 124307 (2014).
[32] D. B. Jones, E. Ali, C. G. Ning, J. Colgan, O. Inglfsson, D. H. Madison, and M. J. Brunger, J. Chem. Phys. **145**, 164306 (2016).
[33] H. Chaluvadi, C. G. Ning, and D. Madison, Phys. Rev. A **89**, 062712 (2014).
[34] X. Ren, S. Amami, K. Hossen, E. Ali, C. G. Ning, J. Colgan, D. Madison, and A. Dorn, Phys. Rev. A **95**, 022701 (2017).
[35] S. B. Zhang, X. Y. Li, J. G. Wang, Y. Z. Qu, and X. Chen, Phys. Rev. A **89**, 052711 (2014).
[36] X. Li, M. Gong, L. Liu, Y. Wu, J. Wang, Y. Qu, and X. Chen, Phys. Rev. A **95**, 012703 (2017).
[37] X. Li, X. Ren, K. Hossen, E. Wang, X. J. Chen, and A. Dorn, Phys. Rev. A **97**, 022706 (2018).